12th International Symposium on Turbulence and Shear Flow Phenomena (TSFP12)
Osaka, Japan, July 19–22, 2022

THE DYNAMICS OF COHERENT STRUCTURES IN A TURBULENT WAKE PAST A SPHERE AT RE=3700

Fengrui Zhang
School for Engineering of Matter,Transport and Energy
Arizona State University
fzhang82@asu.edu

Yulia T. Peet
School for Engineering of Matter,Transport and Energy
Arizona State University
ypeet@asu.edu

ABSTRACT

The turbulent wake flow past a sphere at $Re_D = 3700$ is investigated via Direct Numerical Simulation (DNS). The characteristic motions in the wake flow, such as vortex shedding and bubble pumping are identified by the probes placed in the near wake with a dominating frequency of $St = fu_\infty/D = 0.22$ and 0.004, respectively. The modal analysis is conducted in the wake area using Proper Orthogonal Decomposition (POD) and Dynamic Mode Decomposition (DMD). The vortex shedding and bubble pumping motions are also captured by the modal analysis. The results from POD and DMD show comparable patterns of both characteristic motions. For the bubble pumping motion, the dominating frequency of the corresponding POD mode is $St = 0.004$, while the DMD mode that is directly related to the separation bubble has the frequency of $St = 0.009$.

INTRODUCTION

A turbulent wake forms past a body moving in a fluid flow. It is a canonical phenomenon, yet it impacts many realistic applications, particularly in the transport industry. Thus it is beneficial to understand the physics behind such flows. During the past few decades, turbulent wakes were investigated by both experimental (Achenbach (1974); Berger *et al.* (1990)) and computational (Tomboulides & Orszag (2000); Yun *et al.* (2006); Rodriguez *et al.* (2011)) tools. Characteristic motions of the wake flow such as vortex shedding and bubble pumping were previously identified. In the current work, we intend to characterize temporal spectra and spatial low-dimensional flow patterns associated with these motions in a wake of a sphere.

A wake flow past a sphere with a sub-critical Reynolds number $Re_D = 3700$ has been studied by high-fidelity simulations in recent years (Yun *et al.* (2006); Rodriguez *et al.* (2011); Pal *et al.* (2017)). In this flow, the transition to turbulence occurs in the near wake, which gives rise to rich physical phenomena and interesting flow dynamics. This Reynolds number is also low enough to allow for the use of Direct Numerical Simulations, making the chosen setup as a model for investigation in the current paper. Some of the previous high-fidelity simulation studies with similar flow conditions focused on the power spectral analysis in the wake of the flow, but without further linking the frequencies to the shape and dynamics of coherent structures associated with these frequencies.

In the current paper, we identify the characteristic motions associated with specific frequencies in the wake. Subsequently, with the help of the modal analysis, the characteristic motions are visualized as coherent structures. The results of the Proper Orthogonal Decomposition (POD) and Dynamic Mode Decomposition (DMD) for the identification of these structures are compared.

NUMERICAL METHODS

In the current study, the incompressible Navier-Stokes equations are solved via Direct Numerical Simulations using the open source code Nek5000 (Fischer *et al.* (2015)). A high-order spectral element method (SEM) is employed to discretize the spatial terms. In order to avoid spurious pressure modes, velocity and pressure are approximated with different degree polynomials by a P_N/P_{N-2} method. $N = 5$ is chosen as the polynomial order in the current study. For the temporal discretization, the convection terms are treated explicitly with the second-order extrapolation scheme, while diffusion terms are treated implicitly with the second-order backward difference scheme. SEM is also known for its geometrical flexibility and provides a setup, in which a body-fitted mesh on the spherical model surface is generated with high-order accuracy utilizing N^{th}-order polynomials.

COMPUTATION SET-UP

The DNS of the flow past a sphere at $Re_D = 3700$ is carried out in a cylindrical computational domain with $x \times r \times \varphi = [-5D, 15D] \times [0, 10D] \times [0, 2\pi]$, where D is the sphere diameter. The center of the sphere is located at the origin of the coordinate system. The O-grid mesh with 9.8 million degrees of freedom (DOFs) is utilized for the baseline simulation. The mesh in the boundary layer around the sphere is refined with a minimum element height $\Delta r_{min} = 0.015D$.

A Dirichlet boundary condition with uniform freestream velocity u_∞ is imposed at the inflow boundary. The outer boundaries of the cylindrical domain are treated with stabilized

outflow boundary conditions (Dong *et al.* (2014)). The no-slip wall boundary condition is employed on the sphere surface.

A time step $\Delta t = 0.0016D/u_\infty$ is used in this case with a CFL number around 0.88 for the baseline case (Mesh 2). The initial conditions for the simulation are set up as a uniform velocity and pressure with their corresponding free-stream values. In order to prevent the flow statistics from being affected by the initial transient, the data for analysis is being collected starting at $t = t_{\min} = 200D/u_\infty$. The snapshots are saved every 125 time steps, corresponding to a period between snapshots of $\Delta t_{\text{snap}} = 0.2D/u_\infty$. As a result, a total number of 4400 snapshots (spanning over $\Delta t_{\text{stat}} = 880D/u_\infty$) are collected until $t = t_{\max} = 1080D/u_\infty$.

RESULTS

We first demonstrate the grid convergence of the current simulations and present the results of the validation against the data available in the literature for the flow over a sphere at comparable Reynold numbers. For the grid convergence test, two more meshes were generated: Mesh 1 with the lower number of DOFs (2.8 mln.), and Mesh 3 with the higher number of DOFs (36.7 mln.), as compared to the baseline mesh (Mesh 2 with 9.8 mln. DOFs). The results for the three meshes were compared with the experimental data from Kim & Durbin (1988), and with the numerical data from Seidl *et al.* (1998); Yun *et al.* (2006); Rodriguez *et al.* (2011); Bazilevs *et al.* (2014); and Dorschner *et al.* (2016). All these references used $Re_D = 3700$ as in the current simulations, except for Seidl *et al.* (1998) who used $Re_D = 5000$. Table 1 presents a comparison of the vortex shedding frequency (via $St = fu_\infty/D$), the length of the separation bubble (L_{sep}/D) , the drag coefficient on the sphere (C_{d}), and the angle of the boundary layer separation along the sphere surface (φ_{sep}). Figure 1 documents the distribution of the pressure coefficient and the normalized wall shear stress along the sphere surface, and Figure 2 presents the mean streamwise velocity profiles at several spatial locations in the sphere wake. It can be seen that Nek5000 results are converged for Mesh 2, and a good agreement with the previous data is obtained for all the presented quantities.

We now proceed with analyzing the results of Mesh 2, having demonstrated the grid convergence. Temporally-averaged and instantaneous contours of streamwise velocity at a streamwise-radial symmetry plane at $z = 0$ are shown in Figure 3. A recirculation region (also known as a separation bubble) is formed in the near wake area. In the temporally-averaged plot, the wake is symmetric about the centerline, while in the instantaneous plot the wake shows a wavy pattern.

Two probes are placed in the near wake to further investigate the dynamics of this flow (Figure 3b). Probe 1, at $(x, r, \varphi) = (3.07D, 0, 0)$, is located close to the edge of the recirculation region to capture the bubble pumping motion, manifesting itself as a periodic shrinkage and expansion of the separation bubble (Rodriguez *et al.* (2011)). Probe 2, at $(x, r, \varphi) = (3.07D, 0.54D, 0)$, is located in the shear layer, where the vortex shedding occurs. In order to identify the characteristic frequency of these two motions, the power spectral density is defined as

$$\text{PSD}\,(St) = \left| \int_{t_{\min}}^{t_{\max}} \phi\,(t) \exp\left(\frac{-i\,2\pi(St)u_\infty t}{D} \right) \text{dt} \right|^2 . \quad (1)$$

We can further define the normalized PSD as

$$\text{Normalized PSD}(St) = \frac{\text{PSD}}{\max_{St} \text{PSD}(St)}. \quad (2)$$

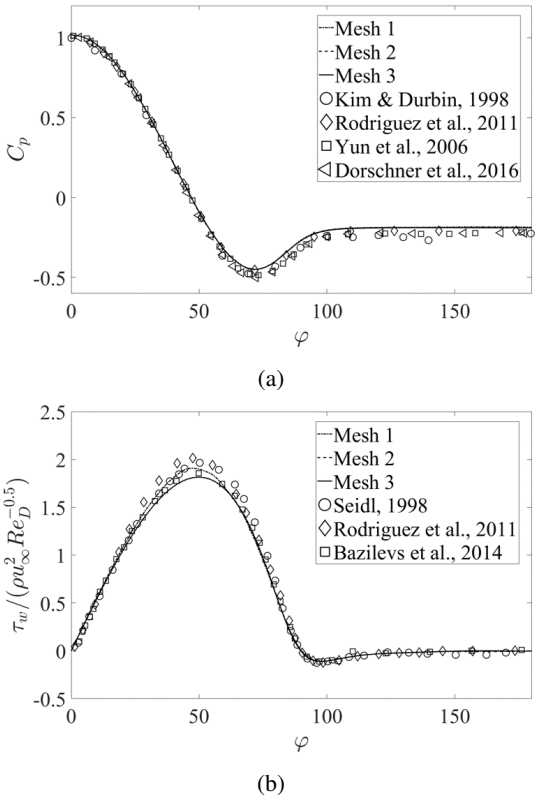

Figure 1: Distribution of the pressure coefficient and normalized wall shear stress along the sphere surface in comparison with available data.

The time series and the corresponding power spectral density of the two probes are plotted in Figure 4. Here ϕ is u', the fluctuating streamwise velocity. For probe 1, the bubble pumping motion is dominated by a low frequency $St = 0.004$. However, we should note that for such a low frequency motion, we only capture 3.5 periods of it in the current simulations. The next strongest peak is at $St = 0.009$, which is approximately half of $St = 0.0178$ identified by Rodriguez *et al.* (2011). The reason for disagreement can be either an insufficient sampling time for this low frequency motion (for $St = 0.009$, the current DNS captures around 8 periods, while for $St = 0.0178$, DNS of Rodriguez *et al.* (2011) captures around 6 periods), or it can be related to a difference in the length of the separation bubble, see Table 1. A longer separation bubble of the current DNS "breathes" with a lower frequency than the shorter bubble in Rodriguez *et al.* (2011). For probe 2, in the high frequency regime, $St = 0.22$ is the dominating frequency, which is the vortex shedding frequency, and it agrees well with the previous studies (Rodriguez *et al.* (2011); Bazilevs *et al.* (2014); Kim & Durbin (1988)). It is interesting to note that the Probe 2 location also feels the low-frequency motion at $St = 0.003$, presumably associated with the bubble pumping.

The coherent structures are illustrated by the contours of the λ_{ci} criterion in Figure 5. It shows that a helical structure is formed in the wake, particularly downstream of the location where vortices are separated from the shear layer. We observe that, as time proceeds (from top to bottom in Figure 5), the vortical structure indicated by the yellow arrow is advecting downstream without rotating about the centerline. Similar findings are also reported in Yun *et al.* (2006) and Rodriguez *et al.* (2011). At the same time, in order to form the helical structure, vortices should shed at different azimuthal locations,

Table 1: Comparison of St, L_{sep}/D, C_{d}, and φ_{sep}, for a flow over a sphere at $Re_D = 3700$ between Nek5000 and other available data. Dash indicates that the data is not available. * DNS of Seidl *et al.* (1998) is performed with $Re_D = 5000$. All other data is for $Re_D = 3700$. LES: Large Eddy Simulations; DNS: Direct Numerical Simulations; LBM: Lattice Boltzmann Method.

Studies	St	L_{sep}/D	C_{d}	$\varphi_{\text{sep}}(^\circ)$
Nek5000 Mesh 1	0.229	2.51	0.381	90.2
Nek5000 Mesh 2	0.219	2.67	0.377	89.9
Nek5000 Mesh 3	0.220	2.70	0.375	89.8
Kim & Durbin (1988) (exp)	0.225	-	-	-
Yun *et al.* (2006) (LES)	0.21	2.62	0.355	90.0
Rodriguez *et al.* (2011) (DNS)	0.215	2.28	0.394	89.4
Bazilevs *et al.* (2014) (DNS)	0.221	2.28	0.392	89.4
Dorschner *et al.* (2016) (LBM)	-	2.51	0.383	90.0
Seidl *et al.* (1998) (DNS*)	-	2.1	0.38	89.5

which must be induced by some rotating mechanism.

In order to "extract" the characteristic motions, such as vortex shedding and bubble pumping, the modal analysis is conducted using the collected snapshots. The modal analysis is performed in a box region identified by a dash line in Figure 3, $x \times y \times z = [0.5D, 10D] \times [-1.5D, 1.5D] \times [-1.5D, 1.5D]$, to focus our attention on the wake area and to lower the computational cost. For that, the flow information is interpolated onto the $101 \times 51 \times 51 = 262701$ uniformly distributed grid points in this box. We first build the matrix $\mathbf{X} \in \mathbb{R}^{n \times m}$ (Taira *et al.* (2017)), where $n = 788103$ is the number of grid points times 3 for the number of dimensions, and $m = 4400$ is the number of snapshots. In this matrix, we have all the three components of the fluctuating velocity at each location in each snapshot. Based on this matrix, we perform POD and DMD decomposition using the techniques outlined in Taira *et al.* (2017), to study the characteristic motions in the wake flow.

The visualization of POD modes and the power spectral analysis of their temporal coefficients is shown in Figure 6. The first two modes are related to the vortex shedding motion with the same dominating frequency of $St = 0.22$. From the spatial pattern of this mode pair, it is clear that the vortex shedding doesn't start from the trailing edge of the sphere; instead, it occurs more than $1.5D$ downstream of the trailing edge. The fifth mode is linked to the motions of the separation bubble with a dominating frequency of $St = 0.004$. The most energetic portion of this mode is located around the separation bubble. Thus, this mode reflects the motion of the whole separation bubble. The third and fourth modes (not shown here) are also dominated by the vortex shedding frequency, but with a noisier pattern.

DMD modes with vortex shedding frequency and bubble pumping frequency are depicted using the fluctuating streamwise velocity in Figure 7. The visualization of vortex shedding motion shows almost identical patterns with the results from the first mode of POD. Figure 7(a) only presents the real part of this DMD mode, the imaginary part depicts similar patterns with the second POD mode. It is because the first two POD modes are dominated by the vortex shedding frequency with a relatively clean spectrum, while a DMD mode is only linked with a single frequency. For the bubble pumping motion, the DMD mode with a frequency of $St = 0.009$ is more asymmetric, but both POD and DMD modes are able to capture the main pattern around the separation bubble. It suggests that both frequencies, $St = 0.004$ and $St = 0.009$, are involved in the bubble pumping motion. The fact that one frequency is essentially twice as high as the other indicates that they may be related as sub- and super-harmonics of the same process.

CONCLUSIONS

Direct numerical simulations are carried out to investigate the wake flow past a sphere at $Re_D = 3700$. The main focus of this paper is to characterize the dynamics of coherent structures that are related to the characteristic motions of the wake flow.

Before conducting analysis of this wake flow, we demonstrate the grid convergence of results and validate them against both experimental and numerical data available in the literature. An overall good agreement is achieved.

For the analysis, we first look at the temporally-averaged and instantaneous contours of the streamwise velocity. Two probes are placed in the near wake region to capture the vortex shedding and bubble pumping motions. A low frequency $St = 0.004$ is identified at probe 1 as the dominating frequency of the bubble pumping motion. For probe 2, the dominating frequency is $St = 0.22$, which is the vortex shedding frequency.

The helical structure of the wake is illustrated by the contour of λ_{ci}. A vortical structure is traced as the time advances. No obvious rotation about the geometric centerline is observed; instead, the structure is merely translating downstream.

To visualize and further investigate the coherent structures that are related to the characteristic motions, we carry out modal analysis using POD and DMD. Both POD and DMD are able to capture the patterns of vortex shedding and bubble pumping. The vortex shedding patterns from both methods are almost identical. For the bubble pumping, the dominating frequency of the corresponding POD mode is $St = 0.004$, and the second peak is at at a higher frequency of $St = 0.009$, while the DMD mode that is related to the bubble pumping has the frequency of $St = 0.009$.

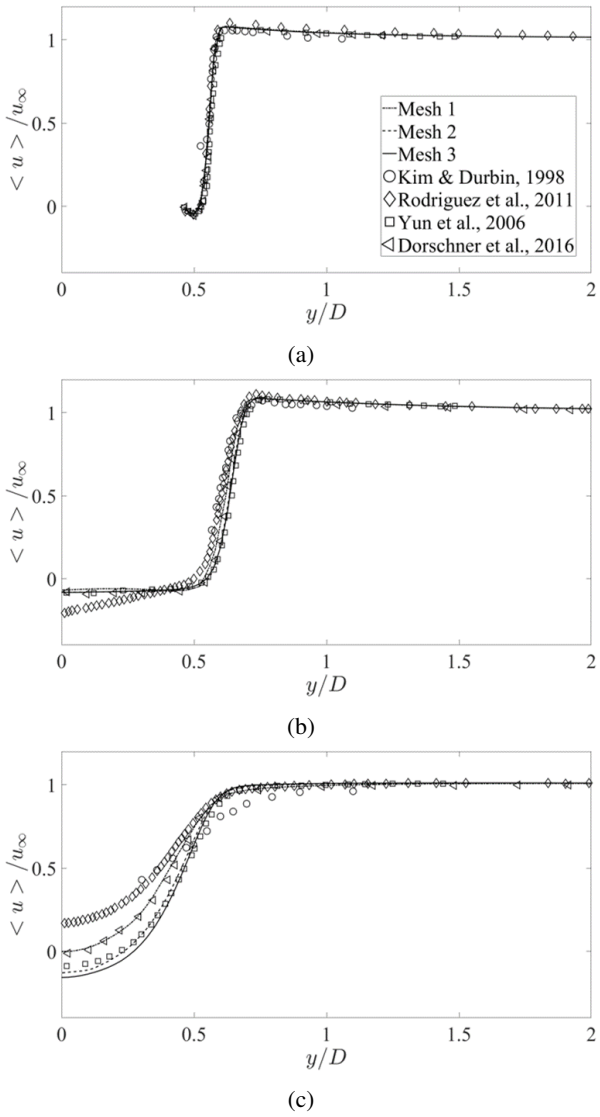

Figure 2: Time-averaged streamwise velocity profiles at (a) $x = 0.2D$, (b) $x = 1.6D$, (c) $x = 3D$, in comparison with available data.

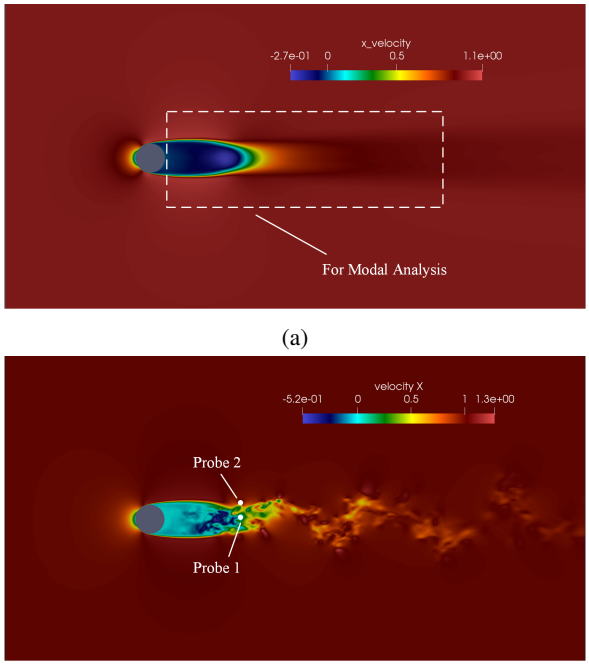

Figure 3: Temporally-averaged (top) and instantaneous (bottom) streamwise velocity contours on the plane $z = 0$.

Acknowledgements

This work is supported by NSF CBET grants # 1707075 and 1944568.

REFERENCES

Achenbach, E. 1974 Vortex shedding from spheres. *Journal of Fluid Mechanics* **62**, 209–221.

Bazilevs, Y., Yan, J., De Stadler, M. & Sarkar, S. 2014 Computation of the flow over a sphere at Re= 3700: A comparison of uniform and turbulent inflow conditions. *Journal of Applied Mechanics* **81** (12), 121003.

Berger, E., Scholz, D. & Schumm, M. 1990 Coherent vortex structures in the wake of a sphere and a circular disk at rest and under forced vibrations. *Journal of Fluids and Structures* **4**, 231–257.

Dong, S., Karniadakis, G. E. & Chrissostomidis, C. 2014 A robust and accurate outflow boundary condition for incompressible flow simulations on severely-truncated unbounded domains. *Journal of Computational Physics* **261**, 83–105.

Dorschner, B., Frapolli, N., Chikatamarla, S. S. & Karlin, I. V. 2016 Grid refinement for entropic lattice Boltzmann models. *Physical Review E* **94** (5), 053311.

Fischer, P., Lottes, J., Kerkemeier, S., Marin, O., Heisey, K., Obabko, A., Merzari, E. & Peet, Y. 2015 Nek5000 User's manual. Technical Report ANL/MCS-TM-351, Argonne National Laboratory, http://nek5000.mcs.anl.gov.

Kim, H. J. & Durbin, P. A. 1988 Observations of the frequencies in a sphere wake and of drag increase by acoustic excitation. *Physics of fluids* **31** (11), 3260–3265.

Pal, A., Sarkar, S., Posa, A. & Balaras, E. 2017 Direct numerical simulation of stratified flow past a sphere at a subcritical Reynolds number of 3700 and moderate Froude number. *Journal of Fluid Mechanics* **826**, 5–31.

Rodriguez, I., Borell, R., Lemkuhl, O. & Oliva, A. 2011 Direct numerical simulation of the flow over a sphere at Re = 3700. *Journal of Fluid Mechanics* **679**, 263–287.

Seidl, V., Muzaferija, S. & Peric, M. 1998 Parallel DNS with local grid refinement. *Appl. Sci. Res.* **59**, 379–394.

Taira, K., Brunton, S. L., Dawson, S. T. M., Rowley, C. W., Colonius, T., McKeon, B. J., Schmidt, O. T., Gordeyev, S., Theofilis, V. & Ukeiley, L. S. 2017 Modal analysis of fluid flows: An overview. *AIAA Journal* **55**, N. 12.

Tomboulides, A. G. & Orszag, S. A. 2000 Numerical investigation of transitional and weak turbulent flow past a sphere. *Journal of Fluid Mechanics* **416**, 45–73.

Yun, G., Kim, D. & Choi, H. 2006 Vortical structures behind a sphere at subcritical Reynolds numbers. *Physics of Fluids* **18**, 015102.

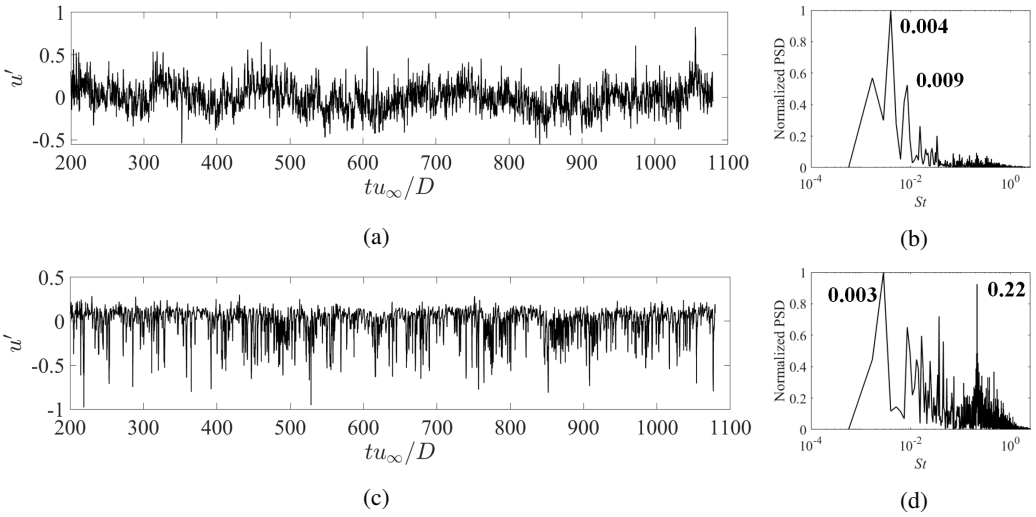

Figure 4: Time series of u' (left) and its power spectral analysis (right) at probe 1 (top) and probe 2 (bottom).

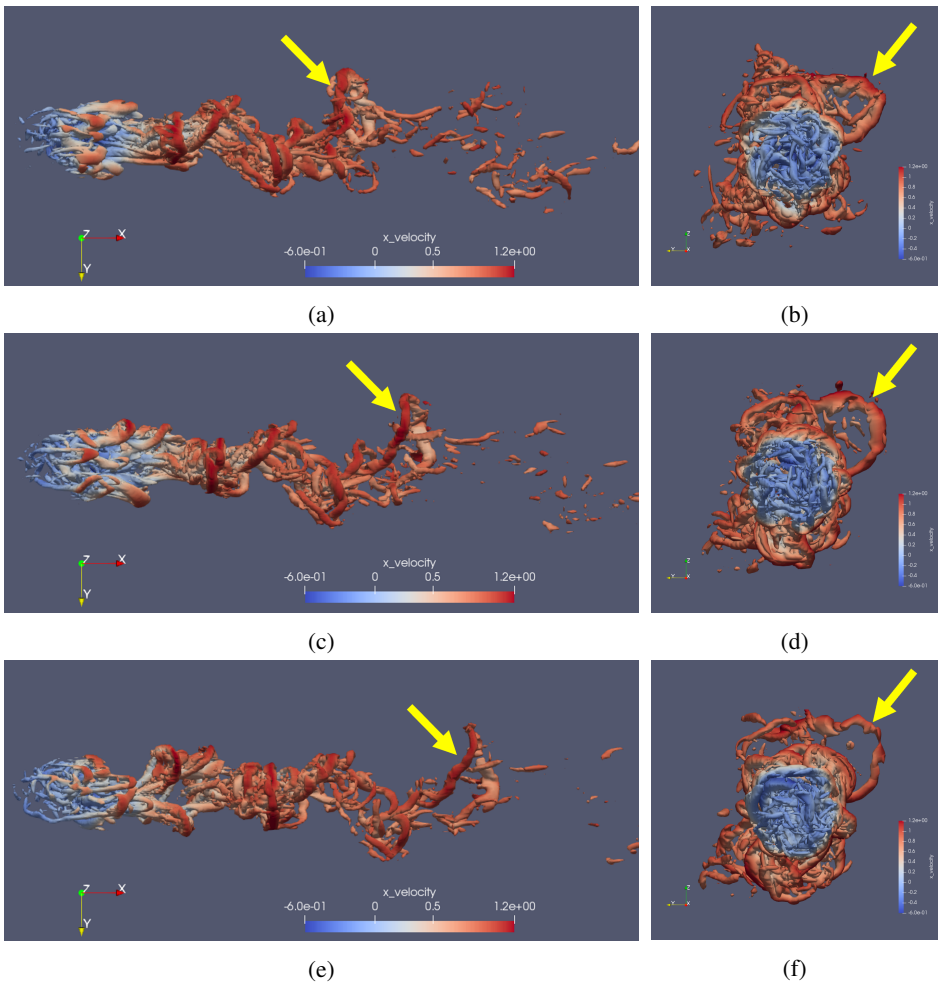

Figure 5: Contour of λ_{ci} with the value of $0.5\,(u_\infty/D)^2$ from (left) view of the streamwise-radial plane; (right) view from upstream. Time advances from top to bottom. Yellow arrow tracks a specific hairpin.

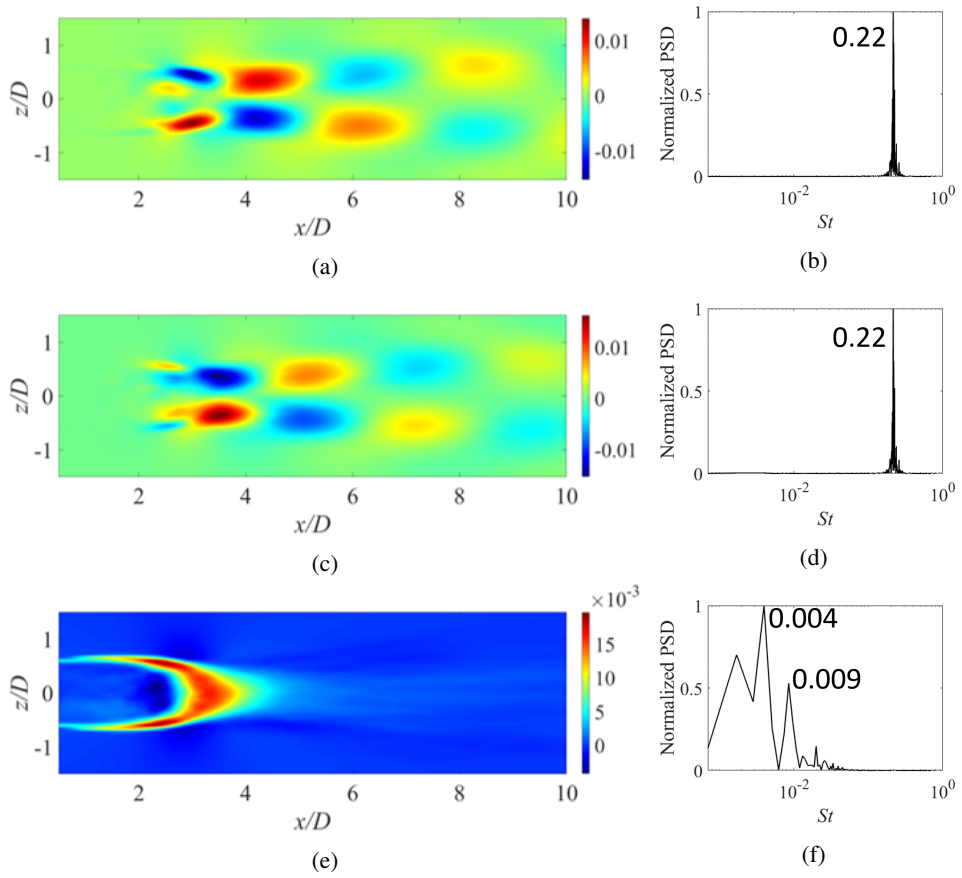

Figure 6: The first (top), second (middle) and fifth (bottom) POD modes on the $z = 0$ plane (left), and power spectral analysis of each mode's temporal coefficient (right). The leftmost edge of each snapshot is at the location of the trailing edge of the sphere ($x/D = 0.5$).

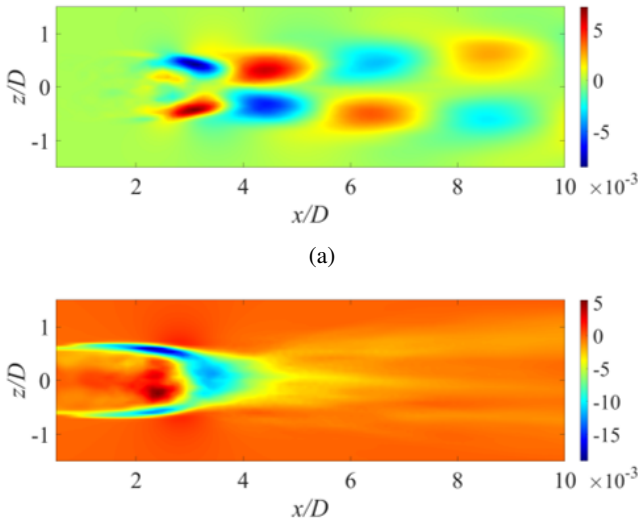

Figure 7: DMD modes with $St = 0.22$ (a) and $St = 0.009$ (b) on the $z = 0$ plane. The leftmost edge of each snapshot is at the location of the trailing edge of the sphere ($x/D = 0.5$).